

# The effect of Pulse profile evolution on Pulsar Dispersion Measure

A. L. Ahuja,<sup>1</sup> D. Mitra,<sup>2</sup> and Y. Gupta<sup>2</sup>

<sup>1</sup> IUCAA, Ganeshkhind, Pune University, Pune, India

<sup>2</sup> National Center for Radio Astrophysics, TIFR, Pune University Campus, Pune 411007, India

Released 2007 Xxxxx XX

## ABSTRACT

In an earlier paper (Ahuja et al. 2005), based on simultaneous multi-frequency observations with the Giant Metrewave Radio Telescope (GMRT), we reported the variation of pulsar dispersion measures (DMs) with frequency. A few different explanations are possible for such frequency dependence, and a possible candidate is the effect of pulse shape evolution on the DM estimation technique. In this paper we describe extensive simulations we have done to investigate the effect of pulse profile evolution on pulsar DM estimates. We find that it is only for asymmetric pulse shapes that the DM estimate is significantly affected due to profile evolution with frequency. Using multi-frequency data sets from our earlier observations, we have carried out systematic analyses of PSR B0329+54 and PSR B1642–03. Both these pulsars have central core dominated emission which does not show significant asymmetric profile evolution with frequency. Even so, we find that the estimated DM shows significant variation with frequency for these pulsars. We also report results from new, simultaneous multi-frequency observations of PSR B1133+16 carried out using the GMRT in phased array mode. This pulsar has an asymmetric pulse profile with significant evolution with frequency. We show that in such a case, amplitude of the observed DM variations can be attributed to profile evolution with frequency. We suggest that genuine DM variations with frequency could arise due to propagation effects through the interstellar medium and/or the pulsar magnetosphere.

**Key words:** miscellaneous – methods:data analysis – pulsars:DM, B0329+54, B1133+16, B1642–03.

## 1 INTRODUCTION

Radio signals from a pulsar undergo dispersion due to the ionized inter-stellar plasma. This effect is characterised by the dispersion measure (DM) of the pulsar. In an earlier paper (Ahuja et al. 2005, hereafter *Paper I*), we described a novel technique for estimation of pulsar DM using the simultaneous multi-frequency observing capability of the GMRT. This technique allows accurate estimates of DM to be obtained at single epochs, without use of absolute timing information. The accuracy of these single epoch DM estimates was shown to be  $\sim 1$  part in  $10^4$  or better, for the bright pulsars.

One of the interesting results reported in *Paper I* is based on the fact that simultaneous dual-frequency observations, at more than one pair of radio frequency bands, were carried out within a short interval of time. As a result, for some of the pulsars studied, we could obtain DM estimates using different pairs of frequency bands, at the same epoch. The results from this showed small but signif-

icant differences in the DM values from different frequency bands, for the pulsars thus studied. This difference was of the same magnitude and sign at different epochs, signifying that it is a systematic effect rather than a random difference that changes with epoch. There have been reports in literature about differences in pulsar DMs estimated from different parts of the radio spectrum (e.g. Shitov et al. 1988; Hankins et al. 1991).

A few different explanations are possible for frequency-dependent DM variations. A likely candidate is the effect of profile shape evolution with frequency (e.g. Phillips & Wolszczan 1992), which can lead to an effective shift of the phase of the pulse at different frequencies, resulting in errors in estimating the dispersion delays between different frequency pairs. On the other hand, physical origins for DM variations with frequency can be found both in the ISM and/or the pulsar magneto-spheric emission processes (e.g. Kardashev et al. 1982).

In this paper, we concentrate on a detailed study to assess the effect of pulse shape evolution on DM estimates of

arXiv:astro-ph/0702440v1 16 Feb 2007

pulsars. In section 2 we discuss the data used for our study as well as discuss the new, simultaneous 4 frequency observations carried out using the GMRT. To examine the role of the effects mentioned above, and to better understand the problem, numerical simulations can provide a powerful tool. The second part of this paper describes such simulations and discusses the conclusions obtained from them.

## 2 DATA AND OBSERVATIONS

To study frequency dependent DM variations, we focus on three bright pulsars - PSR's B0329+54, B1642-03 and B1133+16 - each showing varying degree of profile complexity and pulse shape evolution with frequency. Some useful parameters of these pulsars are given in Table 1. Column 2 of Table 1 contains the formal DM values given in the old pulsar catalog (Taylor, Manchester & Lyne 1993) and the new catalog (Hobbs et al. 2004), while Column 3 of the table displays the mean DM values from *Paper I* and Column 4 gives the pulsar period.

For our study in this paper, we have used single epoch, simultaneous multi-frequency data for PSR's B0329+54 (at 610+320+243 MHz) and B1642-03 (at 610+325 and 325+243 MHz), based on observations reported in *Paper I*. Although the results for PSR B0329+54 reported in *Paper I* used only one dual-frequency observation at each epoch, at three epochs (January 8, January 22 and May 14, 2001) this pulsar was observed at 3 frequency bands simultaneously: 610+320+243 MHz. Using the data from these epochs, we have estimated the DM values for the different frequency pairs. The results for the January 22, 2001 observations give DM values of 26.78610(4) pc cm<sup>-3</sup> for the 610+320 MHz frequency pair, 26.77947(3) pc cm<sup>-3</sup> for the 610+243 MHz frequency pair and 26.77256(5) pc cm<sup>-3</sup> for the 230+243 MHz frequency pair. For PSR B1642-03, using the data from August 18, 2001, we obtain DM values of 35.75809(7) pc cm<sup>-3</sup> for the 610+325 MHz frequency pair and 35.72262(7) pc cm<sup>-3</sup> for the 325+243 MHz frequency pair. For PSR B1133+16, observations reported in *Paper I* had only one frequency pair at each epoch. Hence, to obtain simultaneous multi-frequency data, we made new observations with the GMRT using an improved technique, as described below.

In *Paper I* we described the basic scheme for using the GMRT in a simultaneous dual-frequency pulsar observing mode, as well as the steps involved in processing the data for obtaining accurate estimates of pulsar DMs. As explained there, the crucial aspect of the scheme is that, in order to eliminate all instrumental delays, baseband signals from two different radio frequency bands (coming from two sub-arrays of the GMRT) are added together in one multi-channel pulsar receiver. The dispersion delay of the pulsar signal between the two radio frequency bands is then used for discriminating between the pulses at the two frequency bands. One drawback of this scheme was that the pulsar signals from the two frequency bands could overlap each other, depending on the nature of the dispersion delay track across the 16 MHz of baseband bandwidth of each of the two frequency bands (see *Paper I* for details). This makes it difficult to apply the scheme easily for simultaneous observations using 3 or 4 frequency bands.

To overcome the above limitation, we now use a modified scheme wherein the digital sub-array combiner which does the addition of the multi-channel baseband data from different antennas, is programmed to blank the data for a selected set of frequency channels for antennas from a given sub-array. This is akin to setting non-overlapping filter banks for each sub-array and allows the 16 MHz bandwidth to be divided between the different radio frequency bands of observations, without any overlap between signals from the different bands, while still preserving the time alignment of the data from the different frequency bands. The sub-band for each frequency band can be conveniently placed anywhere in the 16 MHz band, by simply changing the channel mask settings for each antenna of the corresponding sub-array. Using this method, the number of frequency bands for which simultaneous multi-frequency observations can be done is easily extended - it is limited only by the loss of S/N due to the reduction of the effective bandwidth from each frequency band. This loss is compensated to some extent by the fact that in this new scheme, the addition of the data from the different sub-arrays can be carried out in the voltage domain (instead of incoherent addition in the older scheme), allowing the use of phased array mode of operations for each sub-array.

Using the new scheme, we carried out simultaneous observations at four frequency bands of the GMRT - 235, 325, 610 and 1280 MHz - for pulsar B1133+16, on February 3, 2004. The pulsar was found to be weak at 1280 MHz and did not have sufficient signal to noise for reliable DM estimation using this frequency. Hence we restricted our study to 3 frequencies: 235, 325 and 610 MHz. The total bandwidth for each observing frequency band was 4 MHz. The observation was carried out with a sampling interval of 0.256 ms, which is a factor of 2 better than the 0.516 ms used for the observations reported in *Paper I*. The results of the observations give DM values of 4.8098(2) pc cm<sup>-3</sup> for the 610+325 MHz frequency pair, 4.8311(1) pc cm<sup>-3</sup> for the 610+243 MHz frequency pair and 4.8290(2) pc cm<sup>-3</sup> for the 325+243 MHz frequency pair.

## 3 FACTORS AFFECTING DM ESTIMATES

In order to understand the intriguing result of DM varying with frequency, we need to assess the primary factors affecting DM estimates. Let us briefly recall the DM estimation technique which has been described in detail in *Paper I*, and then look into the factors which can produce the observed DM change. Basically, the DM is estimated from the delay in the pulse arrival time  $\Delta t_m$  at two frequencies  $f_1$  and  $f_2$ , and is given by

$$DM = \frac{\Delta t_m}{K \left( \frac{1}{f_1^2} - \frac{1}{f_2^2} \right)} \quad (1)$$

where the constant  $K = 1/(2.410331 \times 10^{-5})$ . All the DM results reported in this paper are based on using the average profile (AP) method described in *Paper I*, where the DM between two simultaneously observed frequency bands is obtained based on estimation of the arrival time delay between the average profiles at the two different frequency bands. As per equation 7 in *Paper I*, the total delay  $\Delta t_m$  can be writ-

**Table 1.** Important parameters of the sample of pulsars.

Pulsar name	Catalogue DM (Old/New) (pc cm <sup>-3</sup> )	Measured mean DM <sup>a</sup> (pc cm <sup>-3</sup> )	Period (sec)
B0329+54	26.776/26.833	26.77870(3)	0.7145
B1133+16	4.8471/4.864	4.8288 (6)	1.1877
B1642-03	35.665/35.727	35.75760(14) <sup>b</sup>	0.3877
B1642-03	35.665/35.727	35.72270(7) <sup>c</sup>	0.3877

<sup>a</sup> see *Paper I*

<sup>b</sup> from frequency pair 610+325 MHz

<sup>c</sup> from frequency pair 325+243 MHz

ten as a combination of 3 terms :  $\Delta t_m = \Delta t_p + \Delta t_i + \Delta t_f$ , where  $\Delta t_p$  is the integral number of pulsar periods in the total delay,  $\Delta t_i$  is the integral number of time samples of delay within a pulsar period, and  $\Delta t_f$  is the fractional sample time component of the delay. One of the main difficulties in estimating the time delays is the lack of knowledge of an appropriate fiducial or reference point in the pulse profiles at different frequencies. In the absence of this, the procedure adopted to find the delay is by cross-correlating the pulse profiles at the two frequency bands. In the AP method,  $\Delta t_p$  is calculated based on the knowledge of the frequencies for the two bands, the catalog DM value and the pulsar period. The value of  $\Delta t_i$  is obtained by finding the lag at which the peak of the cross-correlation occurs. The profile at the lower frequency is then rotated left circularly by this amount to align it with the higher frequency pulse profile. Finally,  $\Delta t_f$  is estimated (refer to Equations 5 to 15 of *Paper I* and the discussion therein for details) from the cross-spectrum,  $CS(\nu)$ , of these aligned profiles. The phase of the cross-spectrum (hereafter CS) can be written as,

$$\phi_{CS}(\nu) = \phi_{2i} - \phi_{1i} + 2\pi\nu\Delta t_f \quad (2)$$

where  $\phi_{1i}$  and  $\phi_{2i}$  are the intrinsic phase functions of the two pulse profiles. Thus, for  $\phi_{1i} = \phi_{2i}$  i.e. when the pulse profiles at the two frequencies have the same shape,  $\Delta t_f = \frac{\Delta\phi_{CS}}{2\pi\Delta\nu}$ . Here,  $\Delta\phi_{CS}$  is the phase change in the cross-spectrum, across an interval of  $\Delta\nu$ .

In the above analysis procedure, the estimated DM can show a frequency dependence if the profile changes significantly with frequency. The effects of these DM changes will be reflected in modified values for  $\Delta t_i$  and/or  $\Delta t_f$ . Now, it is well known that pulse widths at lower frequencies are more than those at higher frequencies – a phenomenon referred to as ‘radius-to-frequency mapping’ (RFM) – see Mitra and Rankin (2002) for a recent review. Furthermore, for several pulsars, pulse shapes at various frequencies can differ significantly (see Rankin 1983). For complex pulse shapes with multiple emission components, the relative strengths of the components, and even the total number of components, can change with frequency. Such pulse shape changes can cause the peak of the amplitude of the cross-correlation function to shift resulting in change in the value of  $\Delta t_i$ . Further, pulse shape variations with frequency can lead to intrinsic pulse phases,  $\phi_{1i}$  and  $\phi_{2i}$ , being different, causing  $\Delta t_f$  to change (see Equation 2). Thus, it is impor-

tant to be able to estimate the magnitude of DM changes due to profile evolution with frequency, before looking for other possible origins for the observed DM changes with frequency. In the next section we describe and present the results of simulations that we have carried out to disentangle the effect of pulse shape evolution on DM estimates.

Before we close this section, it is important to dwell on the issue of the fiducial point in the pulse with respect to which DMs are found. In this aspect, the scheme we have employed here to find the DM is slightly different from most of the previously used techniques. The difference lies in the choice of the fiducial point of the profile. Ideally, to find accurate DMs, the time of arrival estimate of the pulse at different frequencies needs an identifiable feature in the pulse waveform which corresponds to the same rotational phase of the pulsar at each observing frequency. For example, for double component profiles, a number of authors (e.g. Craft 1970; Phillips & Wolszczan 1992) have used the midpoint between the outer peaks as the fiducial point; and for single component profiles, the peak of the pulsar profile is used as the fiducial point. Based on simultaneous observations of pulse micro-structure, Boriakoff (1983) has shown that the micro-structure in a single pulse is not affected by dipolar field line spreading and can be used as accurate fiducial marker for measurement of DMs. Further, for the double component profile pulsar PSR B1133+16, he found that the micro-structure based fiducial marker is in good agreement with the midpoint between conal peaks. In contrast to the above, the CS method that we have used, by its nature, tries to align the profile with respect to the centroid of the pulse. For highly asymmetric profiles the centre and the centroid can be different, thus leading to different DM estimates. The simulations discussed in the next section try to resolve some of these issues.

## 4 SIMULATIONS

With the objective of quantifying the effect of pulse shape variations on DM estimates, we have carried out extensive simulations. The basic paradigm of these simulations is to construct various complex pulse shapes at different frequency bands with a user supplied DM value, pass them through our analysis technique to obtain an output DM value, and compare it with the input DM. Under these con-

trolled situations it is possible to try and pin down the cause for DM changes, at various stages of the analysis.

We have simulated pulse profiles with the observing parameters tuned for the GMRT observations. The following input parameters were used for the simulations: (1) pre-decided pulsar period,  $P$ ; (2) the following information about the frequency bands: (a) frequency band values matching with the real observations, (b) band-width, used in the real observations, (c) number of channels (typically 256) across the band-width, as used in the real observations, (d) side band corresponding to lower side band (USB) or upper side band (LSB), as used in the real observations; (3) time sample bin size,  $T$ ;

At a given frequency, pulse profiles were generated with integral number of time sample bins per period,  $N = \text{nearest integer}(P/T)$ , and hence the effective time sampling was  $T_{eff} = P/N$ .

It is well known that profiles of several pulsars are composed of a number of emission components (Rankin 1993, see). Detailed pulse shape phenomenological studies have revealed that, in general, pulsar emission can be interpreted in the form of a central core emission with nested cones around it (see Mitra & Deshpande 1999). Depending on how the line-of-sight cuts through the emission cone, a given pulse profile might contain an odd number of components where emission from both the cone and core is present, or an even number of components when only the conal emission is seen. Also, the conal emission pairs can have varying intensity and sub-pulse widths. The centre of the core emission is often used as a fiducial point to mark the centre of the profile. Due to aberration and retardation effects, the mid-point of the conal components is expected to lead the centre of the core emission (e.g. Gangadhara & Gupta 2001).

In our simulations, we have used the aforementioned pulsar properties to generate the pulse profiles. Assuming that the emission from the core and the cones have a Gaussian intensity distribution (Kramer et al. 1994), we have generated pulse profiles where the profile is composed of a number of components with each component being a Gaussian function. To generate a profile with a given signal to noise ratio, Gaussian random white noise was added to the signal. Based on the above considerations, the signal at the  $i^{th}$  bin of the profile is calculated as,

$$y(i) = \sum_{j=1}^n [A(j) \times e^{-\frac{(x(i) - \langle x(j) \rangle)^2}{2\sigma(j)^2}}] \quad (3)$$

Here,  $y(i)$  is the  $i^{th}$  bin signal. The index  $j$  refers to the number of peaks in a profile,  $\langle x(j) \rangle$  is position of the  $j^{th}$  peak (centre of the Gaussian),  $A(j)$  is the amplitude of the  $j^{th}$  peak, and  $\sigma(j)$  is the RMS of the  $j^{th}$  peak function.

To produce profiles at multiple frequencies, we have used the conventional wisdom about pulse width evolution properties, where it is generally seen that the overall pulse width scales with frequency  $\nu$  as  $\nu^{-\alpha}$ , where  $\alpha$  is a positive spectral index, with a typical value  $\sim 0.2$  (see Mitra and Rankin 2002). To get the delayed pulse corresponding to an input DM, a fixed fiducial point in the profile needs to be chosen. For profiles with an odd number of components, we have chosen the peak of the central core component as the fiducial point. For profiles with even number of components, the fiducial point was chosen to be the

mid-point of the outer conal component locations. The data generated at the two frequencies were passed through the DM estimation code, to obtain our DM results.

#### 4.1 Simulation results

The simulations were carried out in different steps, starting from a single peak profile without any frequency evolution, and extending to multi-component profiles with significant frequency evolution. Results from the simulation experiments are summarised in Table 2.

The information in the different columns (1 to 8) of this table, is as follows:

1. Experiment number;
2. About the type of profile generated in the experiment;
3. Input DM (in  $\text{pc cm}^{-3}$ );
4. Pulse profile evolution index;
5. Parameters of each component (a Gaussian function): sigma,  $\sigma$  (in ms), amplitude, separation (in ms) of peak from reference point;
6. Total integral number of time samples of delay, fractional sample time component of delay, effective time sample bin size (in ms) and total measured time delay (in s), as estimated from our DM analysis;
7. Output DM (in  $\text{pc cm}^{-3}$ ) from the experiment, with  $1\sigma$  error bar;
8. Deviation of the output DM from the input DM, in units of  $\sigma$ .

All the simulations were carried out for a pulsar with period of 714.5801473327570 ms and DM of 26.776  $\text{pc cm}^{-3}$  respectively<sup>1</sup>. The RMS of the additive noise was kept relatively low (0.015) for the initial experiments (simulation numbers 1 to 4); but in later experiments (simulation numbers 5-10), to see the effect of lower SNR, the input RMS value was increased to 0.05. Profiles were generated at the frequency bands of 610 and 325 MHz. In the analysis, for fitting the phase of the CS with a straight line to estimate the fractional sample time delay, the number of data points used on each side of the 0 frequency channel were  $\sim 20$ .

The simulations presented in Table 2 were carried out systematically, by adding complexities in each successive simulation. Here we discuss the results of 3 simulations in detail, namely simulation numbers 3, 4 and 6, which illustrates the effect of pulse profile evolution on DM estimates. The results of simulation 3 are presented in figure 1. In this case we generated pulse profiles with two symmetrical peaks and the profiles are not evolving in widths with frequency. As is seen in the figure, the corresponding phase function of the CS shows a linear gradient (bottom right panel) as expected, which can be well fit with a straight line to obtain the fractional delay  $\Delta t_f$  with significant accuracy. This is primarily because of the cancellation of the phase function of the Fourier transformed profiles, in the CS phase i.e.

<sup>1</sup> The results obtained from our simulations are independent of these input values. To compare the simulation results with a realistic case, we have used these values which correspond to one of the sample pulsars PSR B0329+54.

**Table 2.** DM results from simulations.

1 <sup>1</sup>	2	3	4	5	6	7	8
1	Single peak, no evolution	26.776	0.00	2.65, 0.055, 0.0	1302, 0.49123, 0.51594, 0.67201	26.77589(13)	-0.837
2	Single peak with evolution	26.776	0.25	2.65, 0.055, 0.0	1302, 0.49227, 0.51594, 0.67201	26.77591(14)	-0.648
3	Symmetric, 2 peaks, no evolution	26.776	0.00	2.65, 0.055, -5.0 2.65, 0.055, 5.0	1303, -0.4957, 0.5159, 0.6720	26.7762(1)	1.67
4	Symmetric 2 peaks, with evolution	26.776	0.25	2.65, 0.055, -5.0 2.65, 0.055, 5.0	1303, -0.4940, 0.5159, 0.6720	26.7762(1)	1.67
5	Asymmetric 2 peaks no evolution	26.776	0.00	1.00, 0.035, -5.0 2.00, 0.055, 5.0	1303, -0.47532, 0.51594, 0.67203	26.77666(34)	1.58
6	Asymmetric 2 peaks, with evolution	26.776	0.25	1.00, 0.035, -5.0 2.00, 0.055, 5.0	1303, 0.3775, 0.5159, 0.6725	26.7941(4)	48.01
7	3 peak symmetric	26.776	0.20	2.300, 0.186, -10.541 12.146, 0.040, 0.0 2.300, 0.186, -10.541	1302, 0.4917, 0.5159, 0.6720	26.7759(1)	-1.06
8	3 peak asymmetric separation	26.776	0.20	2.300, 0.186, -11.249 12.146, 0.040, 0.0 2.300, 0.186, -10.541	1302, 0.4061, 0.5159, 0.6720	26.7741(1)	-18.66
9	3 peak asymmetric separation and sigma	26.776	0.20	2.300, 0.186, -11.249 12.146, 0.040, 0.0 4.019, 0.186, -10.541	1302, -0.2586, 0.5159, 0.6716	26.7605(1)	-150.67
10	3 peak asymmetric separation, sigma and amplitude	26.776	0.20	2.300, 0.186, -11.24941 12.146, 0.040, 0.0 4.019, 0.070, -10.541	1300, 0.0582, 0.5159, 0.6708	26.7259(1)	-415.35

<sup>1</sup>For detail description of the contents in all the columns, see paragraph 2 in Section 4.1

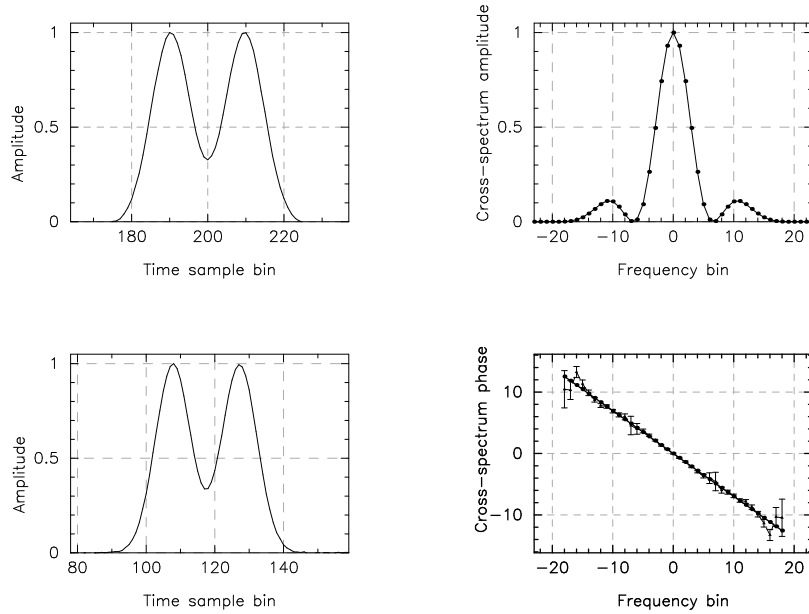


**Figure 1.** Two peaks, symmetric, without evolution, simulated pulse profiles at the two frequencies 325 (left lower panel) and 610 MHz (left upper panel), and the corresponding CS amplitudes (right upper panel) and phase with best fit line (right lower panel).

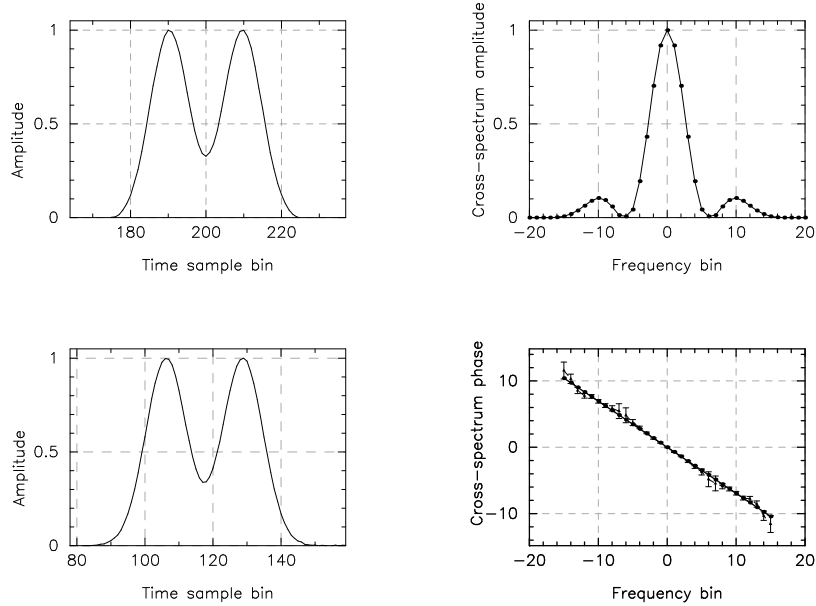


**Figure 2.** The left lower and upper panels represent the two peaks, symmetric, simulated pulse profiles at the two frequencies 325 and 610 MHz, respectively. The corresponding CS amplitude and phase function with best fit are shown in the right upper and lower panels, respectively.

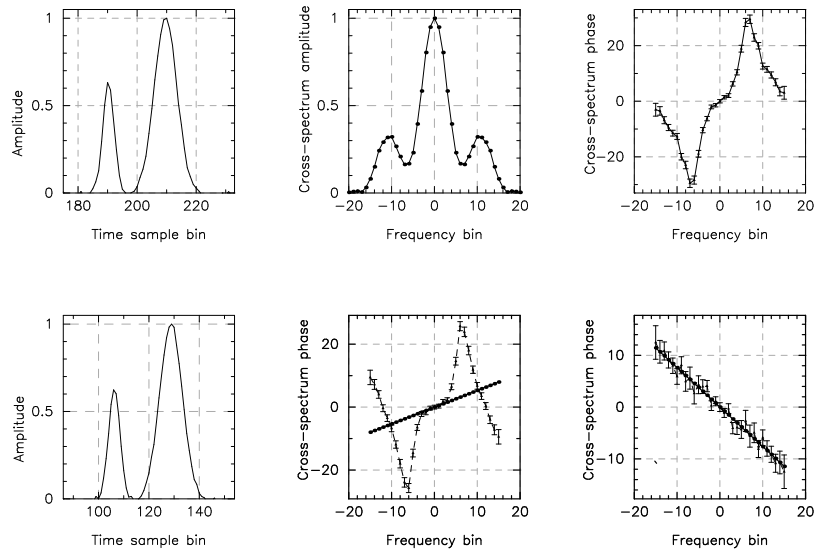


**Figure 3.** The figure shows two peak, asymmetric, with evolution, simulated pulse profiles at two frequency bands 325 (left lower panel) and 610 MHz (left upper panel) respectively. The corresponding CS amplitude (middle upper panel), phase function with best fit line (middle lower panel), template phase function (right upper panel) and template subtracted phase function with best fit line (right lower panel) are shown in the figure.

$\phi_{1i} = \phi_{2i}$  in equation 2. Figure 2 shows the case of simulation 4 where we consider two component, symmetric pulse profiles. The widths of the components and the overall profile evolve with frequency with a spectral index  $\alpha$  of 0.25, with the widths increasing at lower frequencies. Even in this case, the cancellation of the phase functions leads to a linear phase of the CS, allowing for accurate DM estimation. A similar argument holds for simulation numbers 1 through 5 and simulation number 7, as can be seen in Table 2. For all of these cases, the output DM is in good agreement with the input DM.

In simulation 6 two component profiles were generated with a significant degree of asymmetry. The profile and component widths were evolved with frequency with a spectral index of 0.25. Under these circumstance the intrinsic phase function of the profile at each frequency is different and hence the phase function of the CS acquires a complicated phase superposed on the linear gradient due to the fractional delay. This is illustrated in figure 3 where the complexity in the phase function is apparent (bottom middle panel). Attempts to obtain a DM by fitting a straight line to this phase function yield a significantly different value of DM

( $48\sigma$  deviation), as seen in column 8 of Table 2. Results of simulation numbers 8 through 10, where the profiles have 3 components and are asymmetric, given in Table 2), show DM inconsistencies due to similar reasons.

However, if the phase contributions due to the individual pulse profiles are known, it should be possible to subtract these from the CS phase and recover the linear gradient. In the simulations we can do this by creating zero DM profiles using the same fiducial point that has been used to simulate the finite DM profiles. The CS phase for the zero DM profiles is then a measure of the phase function due to the intrinsic pulse shapes. This is shown in the top right corner of figure 3. This phase function, when subtracted from the CS phase of the finite DM profiles, gives back the linear gradient – as shown in the bottom right corner of figure 3. The DM estimated using this gradient is  $26.7752(5) \text{ pc cm}^{-3}$ , and is within  $2\sigma$  of the input DM. This is a significant improvement from the  $48\sigma$  discrepancy, found before correction.

Note that application of the zero DM template phase subtraction technique to real data, needs an assumption for the fiducial point. However, although the profiles are aligned with respect to the fiducial point, the CS method actually finds the DMs by aligning the centroid of the profiles. Thus, for cases where the difference between the fiducial point and the centroid of the profile varies considerably with frequency, the CS method would yield a finite DM even for zero DM aligned profiles. Nonetheless, the template subtracted DM will eventually be based on the choice of the fiducial markers. In principle, for the correct choice of the fiducial marker, the phase subtracted template should recover the linear phase gradient which is solely due to the time delay effect.

In summary, our simulations show that pulse shape evolution, which results in significant differences in the intrinsic phase functions, can affect DM estimates in pulsars.

## 5 FREQUENCY DEPENDENT DM VARIATIONS

Tables 3, 4 and 5 give the DM values obtained for PSR B1642–03, PSR B0329+54 and PSR B1133+16 respectively. Column 1 of these tables (3, 4 and 5) represent the frequency pair used for the DM analysis. Column 2 of the tables provides the information about the DM per bin delay between signals at the two frequency bands. Column 3 gives the DM obtained from the various frequency pairs, and clearly significant DM changes with frequency are seen. In this section we primarily address the question if pulse shape evolution can cause such DM changes.

**PSR B1642-03:** This pulsar has a relatively simple pulse profile and is seen to have a single emission component across frequencies. The lower middle panels of figures 4 and 5 show the phase function of the CS for frequency pairs 610+325 MHz and 325+243 MHz, respectively. The phase function for 610+325 MHz is seen to be linear close to the zero frequency bin, with a sharp bend towards the edge frequencies. A similar trend but with much lower prominence for the sharp bend is seen for the frequency pair 325+243 MHz. To assess if the phase function has any contribution from pulse shape evolution, we have fitted Gaussian components to the profiles and found that the profile is described adequately, at each frequency, by three Gaussians – a cen-

tral dominating Gaussian and two weaker Gaussian on either side, as shown in figure 6. Assuming the peak of the central component to be the fiducial point, we find the zero DM phase functions of the CS to be as shown in the top right panel of figures 4 and 5. Considering these as the template phase functions due to pulse shape evolution, we obtain the template subtracted phase functions as shown in the bottom rightmost panel of these figures. Clearly, we can recover the linear gradient of the phase function which is primarily due to  $\Delta t_f$ . The template subtracted DMs are given in column 5 of Table 3, where we still see a significant change of DM between the two frequency pairs. In analogy with our simulations, since the profile evolution for PSR B1642–03 is relatively symmetric, we find that the template subtracted DM is quite similar to the non template subtracted DM.

For PSR B1642–03 Shitov et al. (1988) reported frequency dependent variation of DM, where the DM observed from low frequency pairs (60 and 102.5 MHz) yielded a value of  $35.736(5) \text{ pc cm}^{-3}$  while higher frequency data (408, 610, 925, 1420 MHz) by Hunt (1971) gave  $\text{DM}=35.665(5) \text{ pc cm}^{-3}$ . Our DM estimates, through restricted over a narrower frequency range, show the opposite trend i.e low frequency pair (325+243 MHz) showing larger DM compared to the value from the higher frequency pair (610+325 MHz). The magnitude of the DM variation is only a factor of 2.2 less than that estimated by Shitov et al. (1988). Since the data used by Shitov et al. (1988) is spaced over 17 years and can be influenced by the temporal DM changes in the ISM, we believe that their conclusion about the observed DM variation is less robust.

**PSR B0329+54:** This is a multicomponent pulsar with a strong central component and weak outriders. As seen in figures 7, 8 and 9, the phase function of the CS shows a significant oscillatory behaviour riding on a linear gradient. The profile is well fitted by five Gaussians, at all the frequencies, as shown in figure 10. Using the peak of the central component as the fiducial point, and performing a similar exercise of finding the zero DM phase template and subtracting it from the actual phase of the CS, we find that the resultant phase shows the distinct linear gradient, as illustrated in the rightmost bottom panels of figures 7, 8 and 9. There is some residual oscillatory behaviour left at a lower level towards the edge frequency bins, which could be attributed to our inadequacy to fit the profile exactly with Gaussian components. In Table 4, the DM values quoted in columns 3 and 5 before and after template subtraction, respectively, however are very similar and show a significant dependence with frequency. The similarity of the DM values are possibly due to the fact that PSR B0329+54 has a very strong central component which dominates any other structure in the pulse. Hence the phase function of the CS close to the central frequency bins (as seen in the bottom middle panels of figure 7, 8 and 9) has the characteristic linear gradient with small errors and hence the straight line fit to the phase responds primarily to this linear gradient. Alternatively, since the central component is a dominating component and we think that the fiducial point lies at the peak of the component, we can put a window only on the central component and use only the windowed region of the pulse to estimate the DM. In this method the corruption of the phase function of the CS will be significantly reduced, since now we are dealing with only a single component which evolves

**Table 3.** DM results for PSR B1642–03 observed at two pairs of frequency bands 610+325 and 325+243 MHz, at one of the epoch, August 18, 2001.

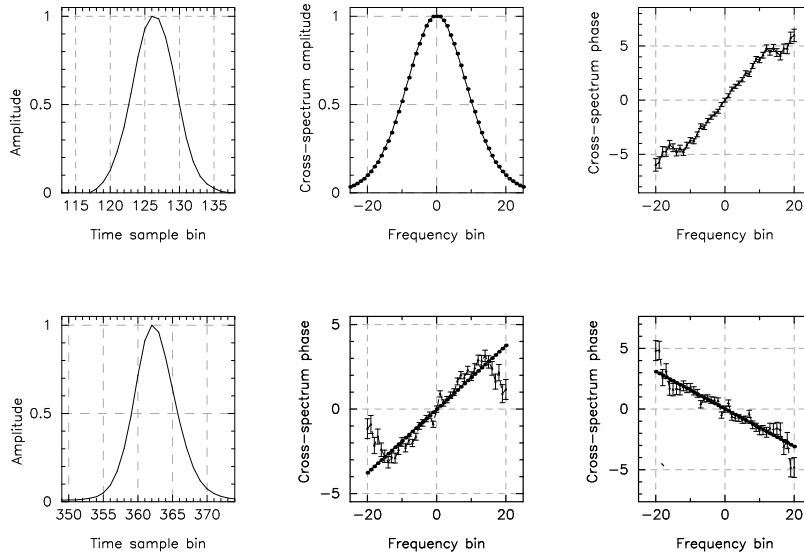
Frequency Combination MHz	DM/bin pc cm <sup>-3</sup> /bin	DM ( $\sigma$ ), before template subtraction pc cm <sup>-3</sup> (pc cm <sup>-3</sup> )	$\Delta DM$ ( $\Delta$ bin) pc cm <sup>-3</sup> (#bin)	DM ( $\sigma$ ), after template subtraction pc cm <sup>-3</sup>	$\Delta DM$ ( $\Delta$ bin) pc cm <sup>-3</sup> (#bin)
610+325	0.02058	35.75809(7)	0.00000 ( 0.000)	35.75308(9)	0.000 ( 0.000)
325+243	0.01493	35.72262(7)	-0.03547 (-2.377)	35.72125(9)	-0.032 (-2.133)

**Table 4.** DM results for PSR B0329+54 observed simultaneously at three frequency bands 243, 320 and 610 MHz, on January 22, 2001

Frequency Combination MHz	DM/bin pc cm <sup>-3</sup> /bin	DM ( $\sigma$ ), before template subtraction pc cm <sup>-3</sup> (pc cm <sup>-3</sup> )	$\Delta DM$ ( $\Delta$ bin) pc cm <sup>-3</sup> (#bin)	DM ( $\sigma$ ), after template subtraction pc cm <sup>-3</sup>	$\Delta DM$ ( $\Delta$ bin) pc cm <sup>-3</sup> (#bin)
610+320	0.01724	26.78610(4)	0.00000 ( 0.000)	26.78404(6)	0.00000 (00.000)
610+243	0.00865	26.77947(3)	-0.00663 (-0.766)	26.77784(4)	-0.00620 (-0.717)
320+243	0.01734	26.77256(5)	-0.01360 (-0.784)	26.77161(7)	-0.01243 (-0.717)

**Table 5.** DM results for PSR B1133+16 observed simultaneously at four frequency bands 227, 325, 610 and 1280 MHz, on February 3, 2004. Data analysed at 3 frequency bands.

Frequency Combination MHz	DM/bin pc cm <sup>-3</sup> /bin	DM ( $\sigma$ ), before template subtraction pc cm <sup>-3</sup> (pc cm <sup>-3</sup> )	$\Delta DM$ ( $\Delta$ bin) pc cm <sup>-3</sup> (#bin)	DM ( $\sigma$ ), after template subtraction pc cm <sup>-3</sup>	$\Delta DM$ ( $\Delta$ bin) pc cm <sup>-3</sup> (#bin)
610+325	0.0101	4.8098(2)	0.0000 (0.000)	4.8547(3)	0.0000 ( 0.000)
610+227	0.0043	4.8311(1)	0.0213 (4.958)	4.8521(2)	0.0026 (-0.605)
325+227	0.0074	4.8290(2)	0.0192 (2.597)	4.8501(3)	0.0046 (-0.619)

**Figure 4.** Pulse profiles for PSR B1642–03, observed simultaneously at 610 (left upper panel) and 325 MHz (left lower panel) bands. Corresponding CS amplitude (middle upper panel), phase function before template subtraction with best fit line (middle lower panel), CS phase for zero DM fitted template (right upper panel) and CS phase function with best fit after template subtraction (right lower panel).



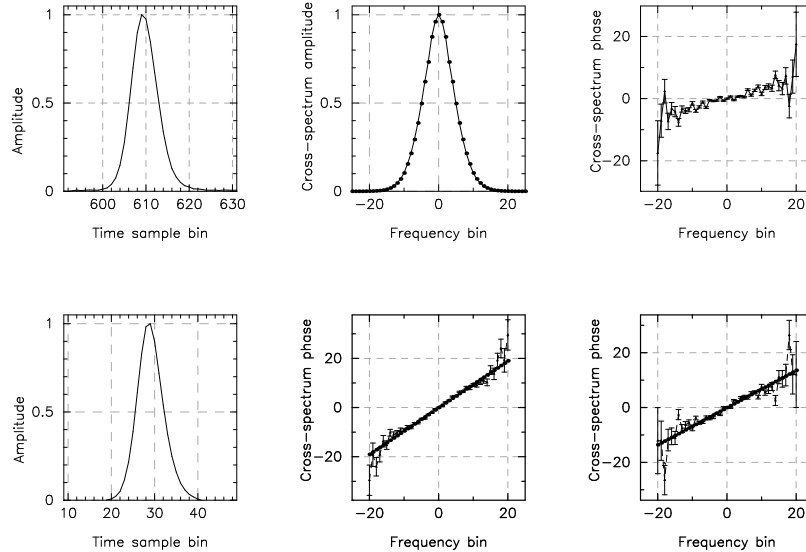


**Figure 5.** Pulse profiles for PSR B1642–03, observed simultaneously at 325 (left upper panel) + 243 MHz (left lower panel) bands. Corresponding CS amplitude (middle upper panel), phase function before template subtraction with best fit line (middle lower panel), CS phase for zero DM fitted template (right upper panel) and CS phase function with best fit after template subtraction (right lower panel).

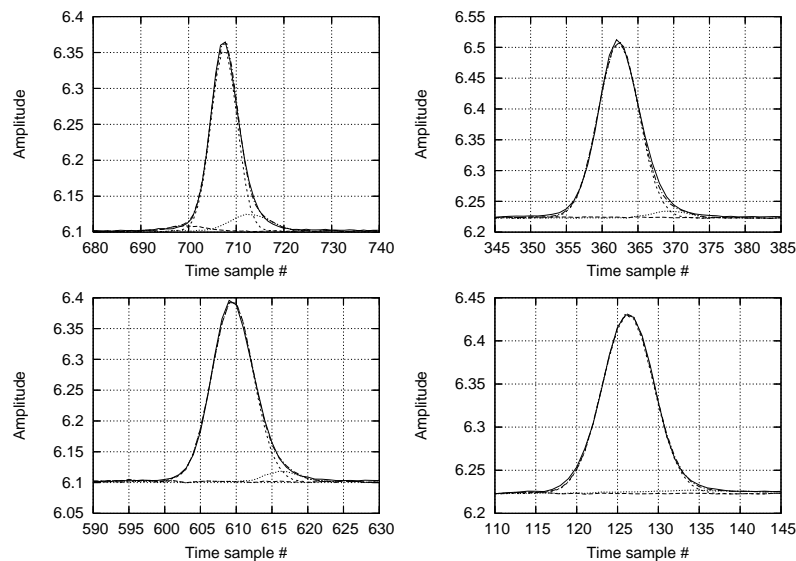


**Figure 6.** Real and fitted pulse profiles, with all the fitting components, for PSR B1642–03, observed at two frequency bands pairs (simultaneously at each): 325 (left lower panel) + 243 MHz (left upper panel), and 610 (right lower panel) + 325 MHz (right upper panel) bands.

more or less symmetrically with frequency. We have applied this technique to the data and found the phase function of the CS to become more linear, however the corresponding DMs found were comparable to values quoted in column 5 of Table 4. For PSR B0329+54 we find a similar trend like PSR B1642–03, where the high frequency pairs give larger DMs compared to low frequency pairs. For PSR B0329+54, as far as we know, no such DM variation study has been reported earlier.

**PSR B1133+16:** The profile of this pulsar shows a great deal of asymmetry, with two prominent conal components of different intensity level, present along with a central

bridge of emission. The conal components vary significantly with frequency also, and this results in a complicated phase function of the CS, similar to what we have encountered in our simulation experiment number 6 earlier (see Table 2). The DM estimates between frequency pairs vary significantly, with estimated fractional time sample bin delays exceeding a few integer bins (for e.g. 4.985 bin for the frequency combination 610+227 MHz, as seen in column 4 of Table 5). Such large changes in DM are clearly due to the complicated phase function of the CS as seen in the bottom middle panels of figures 11, 12 and 13. The phase function in each case has a significant amount of ringing or oscillatory

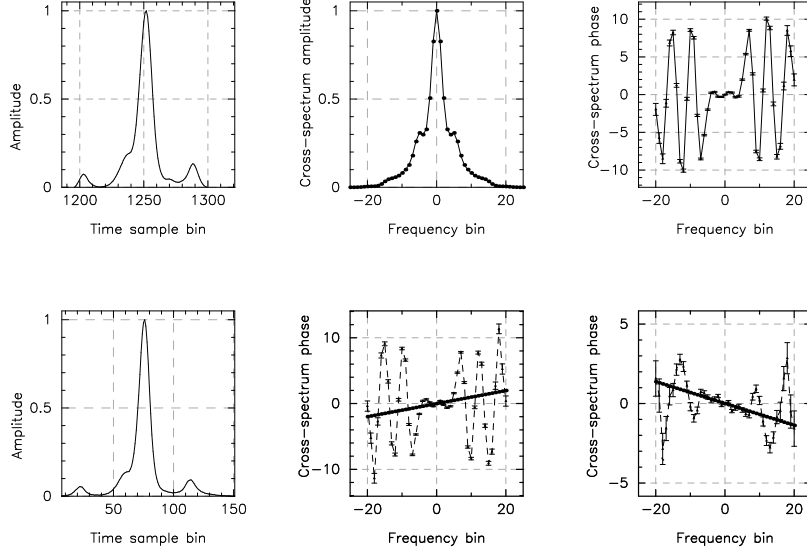


**Figure 7.** Pulse profiles for PSR B0329+54, observed simultaneously at 610 MHz (left upper panel), 320 MHz (left lower panel), & 243 MHz bands. Corresponding to 610+320 MHz CS amplitude (middle upper panel), phase function before template subtraction with best fit line (middle lower panel), CS phase for zero DM fitted template (right upper panel) and CS phase function with best fit, after template subtraction (right lower panel).

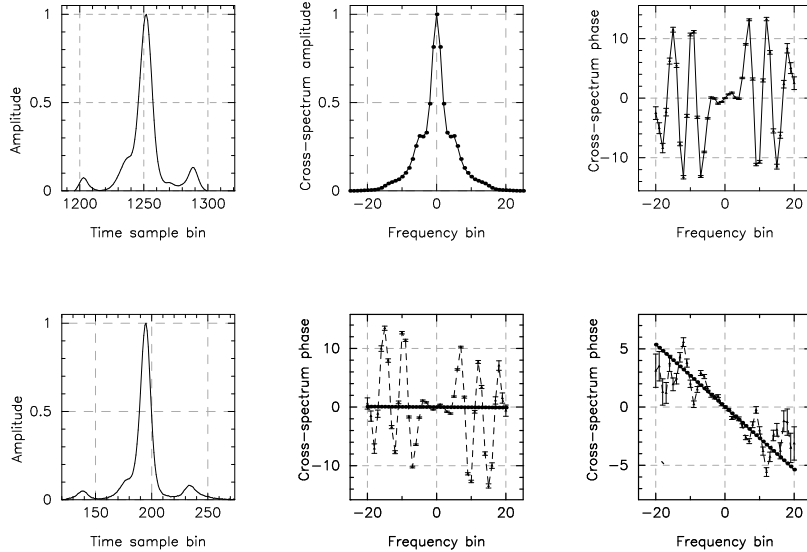


**Figure 8.** Pulse profiles for PSR B0329+54, observed simultaneously at 610 (left upper panel), 320 & 243 MHz (left lower panel) bands. Corresponding to 610+243 MHz CS amplitude (middle upper panel), phase function before template subtraction with best fit line (middle lower panel), CS phase for zero DM fitted template (right upper panel) and CS phase function with best fit, after template subtraction (right lower panel).

behaviour, and attempts to fit straight lines to the data are clearly unsatisfactory.

To understand this large discrepancy we again attempt to estimate the intrinsic phase function of the CS due to pulse shape variations. The pulse profiles at each frequency is adequately fitted by five Gaussians (see figure 14). Since there is no clear central core component in this pulsar, the choice of the fiducial point to produce the template phase function by aligning the profiles at zero DM is tricky. However by choosing the peak of the centrally placed Gaussian (third Gaussian from left), we obtain the zero DM template

and the template subtracted DM as shown in the top and bottom right panels of figures 11, 12 and 13, respectively. The DM differences obtained based on fitting the template subtracted phase functions are far less varying with frequency as seen in columns 5 and 6 of Table 5) (less than an integer bin). It is indeed remarkable that by choosing the central point in the profile we are able to get reasonable DM values between frequencies. However, since the resultant template subtracted phase functions are not entirely linear, we are not certain if the finer DM difference seen in column 5 of the table are real or still corrupted by the in-

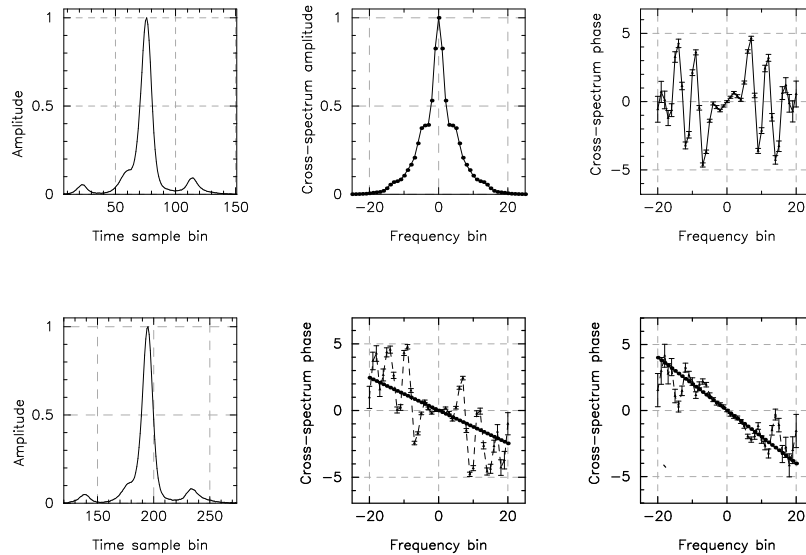


**Figure 9.** Pulse profiles for PSR B0329+54, observed simultaneously at 610 , 320 (left upper panel) & 243 MHz (left lower panel) bands. Corresponding to 320+243 MHz observation CS amplitude (middle upper panel), phase function before template subtraction with best fit line (middle lower panel), CS phase for zero DM fitted template (right upper panel) and CS phase function with best fit, after template subtraction (right lower panel).

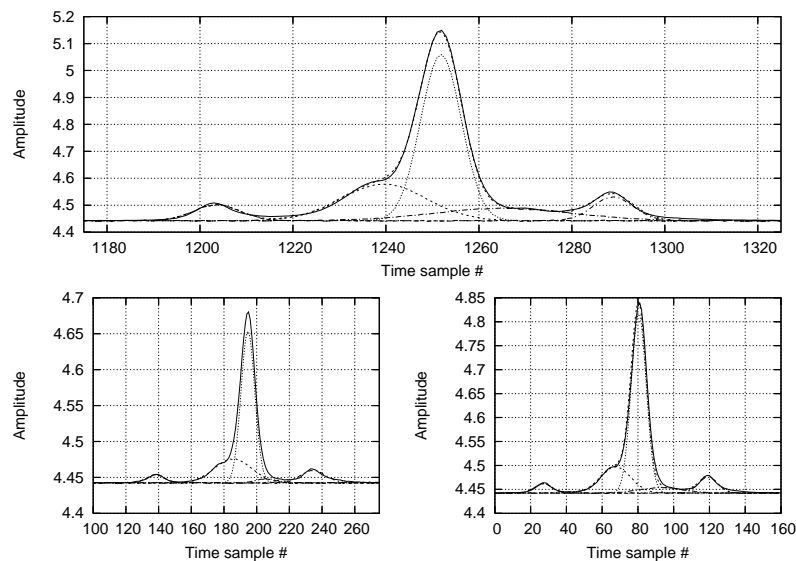


**Figure 10.** The above figure shows pulse profiles for PSR B0329+54, observed on January 22, 2001, simultaneously at three frequency bands 243 (left lower panel), 320 (right lower panel) and 610(upper panel). The dashed lines show all the fitted components and the final fitted profile.

trinsic phase function. We have also tried by choosing a few other points in the profile as the fiducial points, but do not find any better convergence in the DM values with frequency pairs.

PSR B1133+16 has been a subject of several multi-frequency DM studies. Based on alignment of micro-structure in the pulse Borikoff (1983) and Hankins et al. (1991) obtained a  $DM = 4.8460(1) \text{ pc cm}^{-3}$  (from frequencies 318 and 111 MHz) while Popov et al. (1987) obtained  $DM=4.8413(1) \text{ pc cm}^{-3}$  (using three frequencies taken pairwise between 103, 79 and 68 MHz). By alignment of multi-frequency average profile data using the midpoint of the

outer conal pair as a fiducial marker Hankins et al. (1991) found  $DM=4.8470(3) \text{ pc cm}^{-3}$  (based on frequency ranging from 24.8 MHz to 4870 MHz) and Phillips & Wolszczan (1992) observed  $DM=4.8471(2) \text{ pc cm}^{-3}$ , where the observed DMs were slightly larger than that obtained from the micro-structure methods. The DM values reported by us in Table 5 are larger than the previously quoted value, which could be a result of temporal variation of DM in the ISM, and is significantly larger than the micro-structure based DM. The old and new catalog value quoted in Table 1 also shows a significant variation and supports this hypothesis of temporal variation. Shitov et al. (1988) claimed that the

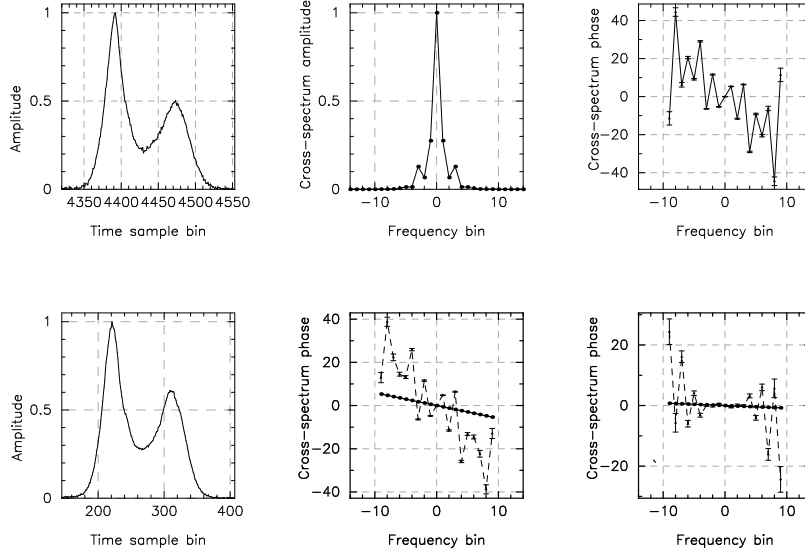


**Figure 11.** Pulse profiles and intermediate results for PSR B1133+16 observed simultaneously at four frequencies. Pulse profiles at 610 (left upper panel) + 325 MHz (left lower panel), corresponding CS amplitude (middle upper panel), phase function before template subtraction with best fit line (middle lower panel), CS phase for zero DM fitted template (right upper panel) and CS phase function with best fit, after template subtraction (right lower panel).

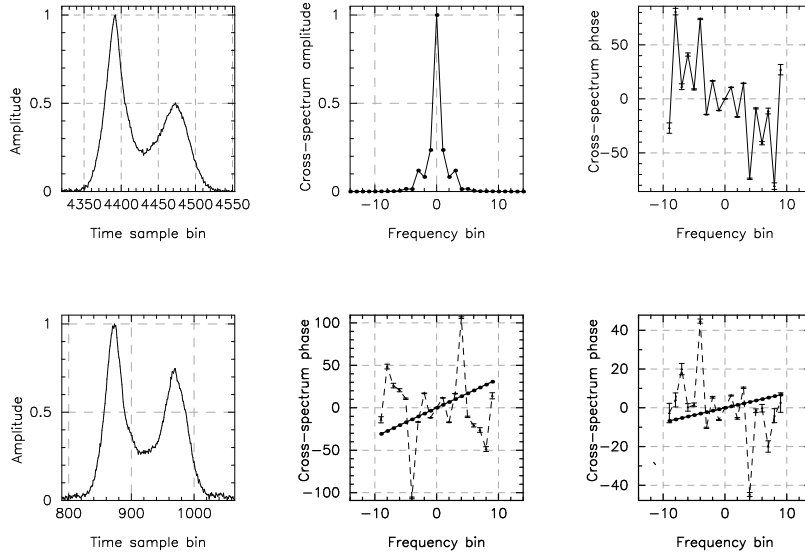


**Figure 12.** PSR B1133+16 observed simultaneously at four frequencies. Pulse profiles at 610 (left upper panel) + 227 MHz (left lower panel), corresponding CS amplitude (middle upper panel), phase function before template subtraction with best fit line (middle lower panel), CS phase for zero DM fitted template (right upper panel) and CS phase function with best fit, after template subtraction (right lower panel).

low frequency pulses showed higher DM values compared to high frequencies, which however was later disputed by Phillips (1991) who found that the pulse arrival times were consistent with the cold plasma dispersion law. Because of the complexity in finding finer changes in DMs as mentioned earlier, and a smaller frequency coverage of our data set, we are unable to comment any more conclusively on this matter, based on our analysis.

## 6 DISCUSSION AND CONCLUSIONS

Earlier studies regarding the existence of frequency dependent DM variations in pulsars have resulted in very different conclusions. Based on multi-frequency data and pulsar timing analysis, Craft (1970) and Phillips & Wolszczan (1992) have shown that pulsar DMs obey the cold plasma dispersion law given by equation 1. On the other hand Shitov and Malofeev (1985), Kuzmin (1986) and Shitov et al. (1988) claim that DMs at low frequencies are systematically larger than DMs at high frequencies. This phenomenon usually goes by the name ‘super dispersion’,

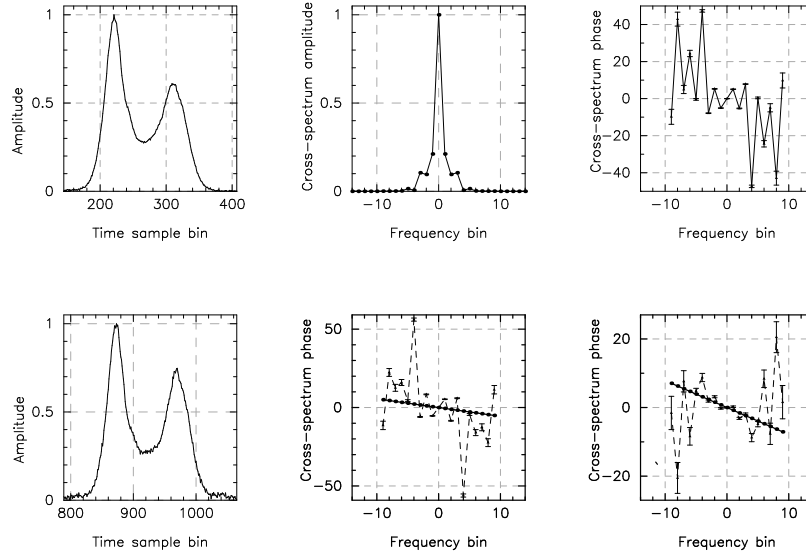


**Figure 13.** Pulse profiles at 325 (left upper panel) + 227 MHz (left lower panel) for PSR B1133+16, observed simultaneously at four frequencies. Corresponding CS amplitude (middle upper panel), phase function before template subtraction with best fit line (middle lower panel), CS phase for zero DM fitted template (right upper panel) and CS phase function with best fit, after template subtraction (right lower panel).

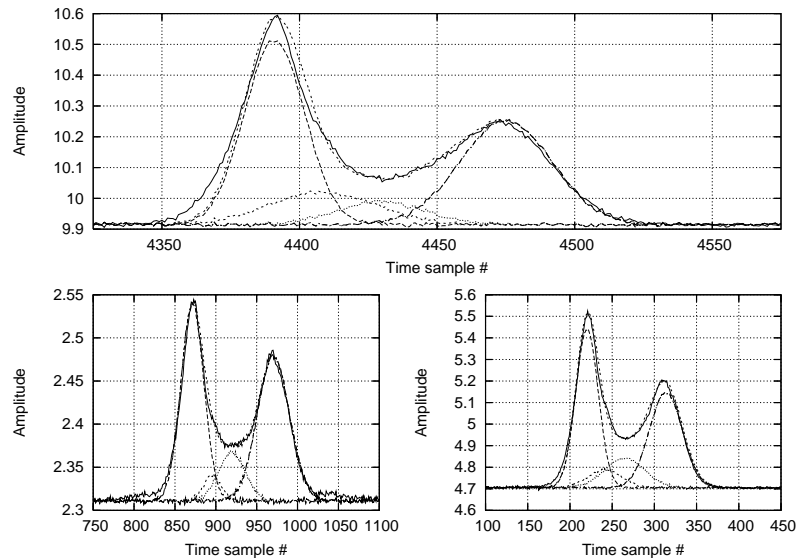


**Figure 14.** The above plot shows pulse profiles for PSR B1133+16 observed on February 3, 2004, simultaneously at three frequency bands 227 (lower left panel), 325 (lower right panel) and 610 MHz (upper panel). The dashed line shows all the fitted components and the final fitted profile at the three frequency bands.

and was explained as magnetic field sweep back in the pulsar magnetosphere. Phillips & Wolszczan (1992) have claimed departure from equation 1 at high frequencies, for two pulsars. As pointed out by Phillips (1991), the comparison of high and low frequency DMs is often based on non simultaneous data and hence the DMs obtained at different frequencies may differ due to temporal DM variability caused by the ISM. Another plausible cause for DM changes claimed by different observers might be due to the choice of fiducial point, used in the analysis to find the DM, not being uniform or consistent.

Results presented in this paper and *Paper I* are based

on simultaneous observations of the frequency pairs for PSR B1642–03 (where the two frequency pairs are observed within typically half an hour interval), and three and four frequency simultaneous observation for PSR B0329+54 and B1133+16. Hence, these are not affected by temporal changes in the ISM. Our DM analysis technique and high sensitivity of the GMRT allows us to obtain DMs, with an accuracy of 1 part in  $10^4$ , which is either comparable or better than accuracies obtained from previous studies. In this paper we have considered the possibility that pulse shape evolution with frequency can affect DM estimates, resulting in pseudo DM variations. We have devised a zero DM

template subtraction method to eliminate this effect and still found that DM for our sample pulsars varies with frequency, to some extent. This variation is seen for all the epochs of observations for PSR B1642–03 (for e.g. see Figure 5 in *Paper I* which shows the DM variation results for B1642–03 for several epochs) and PSR B0329+54. For both these pulsars the DMs obtained from low frequency pairs are less than the higher frequency pairs. In both these cases we have chosen the peak of the pulse profile (by a Gaussian fitting procedure) as the fiducial marker. In the case of PSR B1133+16 we found that pulse shape evolution can affect DM estimates by significant amount. While our zero DM template subtraction method could produce gross correction of the DM values, resulting in matching DMs between frequency pairs at a level of in 1 part in  $10^{-2}$ , the differences are still significant w.r.t the errors in estimation. However our subtraction method is not accurate enough to claim that these variations are real.

We believe that we have established with certainty that PSR B1642–03 and PSR B0329+54 show DM variation with frequency where high frequency DM pairs show higher DM than the low frequency pairs. This effect is opposite to ‘super dispersion’ claimed by several authors (e.g. Shitov et al. 1988). Physically, DM variation with frequency can result both due to the ISM (e.g. Ramachandran et al. 2006) and the pulsar magnetosphere. For a uniform medium in the ISM, dispersion depends on the column density of electrons along the line of sight from the source to the observer. However for a turbulent ISM, due to refractive effects, the emission from the source performs multi-path propagation causing the effective DM to vary. Since pulsar beams at lower frequencies are larger than at higher frequencies, the geometry for multi-path propagation and distribution of the turbulent features becomes a function of frequency, resulting in DM variation with frequency. In such a case, the sign of the DM change with frequency is unpredictable. Another related ISM effect which can cause DM variation is connected to the change of the pulsar waveform due to scatter broadening. Scattering causes the intrinsic emission from the pulsar to be convolved with the response function (typically observed to have an exponential form) of the ISM. Since scattering is a strong function of frequency  $\nu^{-4.4}$  (see Ramachandran et al. 1997, and references therein), the fiducial marker in the pulse profile, tends to arrive later at lower frequencies. This effect will cause DMs to be larger at lower frequencies, quite opposite to what we observe, and hence can be ruled out as a possible explanation for DM variation for PSR B1642–03 and B0329+54.

Alternatively, the emission process and propagation effects in the pulsar magnetosphere can give rise to frequency dependent DM variations. Our observations suggest that the fiducial markers tend to arrive earlier at lower frequencies. For both PSR B1642–03 and B0329+54 the fiducial point is chosen to be the peak of the central core emission which is thought to lie in the plane containing the rotation axis and the magnetic axis. If we assume that RFM operates for core emission in pulsars, then progressively lower frequencies are emitted from higher heights above the neutron star surface. For such an emission process, aberration can cause the low frequency emission to arise at earlier rotation phase compared to the higher frequencies. Such an effect can give rise to DM dependent frequency variations. Combination of

RFM and presence of dispersive plasma in the pulsar magnetosphere can introduce differential shifts in the pulse profile as a function of frequency.

Currently more observations are needed both over a wider frequency range and for a number of pulsars to constrain the nature of frequency dependent DM variations in pulsars. Also further progress in pulsar emission and propagation theories are needed to understand these effects.

**Acknowledgments:** We would like to thank Ajit Kembhavi for his co-operation. We would also like to thank M. Kramer for providing us his Gaussian fitting program which is used extensively in this work. We would like to thank the staff at the GMRT for making the observations possible. The GMRT is run by the National Centre for Radio Astrophysics.

## REFERENCES

- Ahuja, A. L., Gupta, Y., Mitra, D., Kembhavi, A., 2005, *MNRAS* **357**, 1013.  
 Boriakoff, V., 1983, *ApJ* **272**, 687.  
 Craft, H. D., 1970, *PhD thesis, Cornell University*.  
 Gangadhara, R. T., and Gupta, Y., 2001, *Apj* **555**, 31.  
 Hankins, T. H., Izvekova, V. A., Malofeev, V. M., Rankin, J. M., Shitov, Y. P., and Stinebring, D. R., 1991, *ApJ* **373**, L17.  
 Hobbs, G., Lyne, A. G., Kramer, M., Martin, C. E. and Jordan, C. A., 2004, *MNRAS* **353**, 1311.  
 Hunt, G. C., 1971, *MNRAS* **153**, 119.  
 Kardashev, N. S., Nikolaev, N. Ya., Novikov, A. Yu., Popov, M. V., Soglasnov, V. A., Kuzmin, A. D., Smirnova, T. V., Bartel, N., Sieber, W., and Wielebinski, R., 1982, *A&A*, **109** 340.  
 Kramer, M., Wielebinski, R., Jessner, A., Gil, J. A. & Seiradakis, J. H., 1994, *A&AS*, **107**, 515.  
 Kuzmin, A. D., 1986, *Sov. Astron. Lett.* **12**(5), 325.  
 Mitra, D. and Deshpande, A. A., 1999, *A&A* **346**, 906.  
 Mitra, D. and Rankin, J. M., 2002, *ApJ* **577**, 322.  
 Phillips, J. A., 1991, *ApJ* **373L**, 63.  
 Phillips, J. A., and Wolszczan, A., 1992 *ApJ* **385**, 273.  
 Popov, M. V., Smirnova, T. V., Soglasnov, V. A., 1987, *Sov. Astron.* **31**, 529.  
 Ramachandran, R., Demorest, P., Backer, D. C., Cognard, I., Lommen, A., 2006, *astro-ph*, **0601242**.  
 Ramachandran, R., Mitra, D., Deshpande, A. A., McConnell, D. M., and Ables, J. G., 1997, *MNRAS* **290**, 260.  
 Rankin, J. M., 1983, *ApJ* **274**, 359.  
 Rankin, J. M., 1993, *ApJ* **405**, 285.  
 Shitov, Yu. P. and Malofeev, V. M., 1985, *Sov. Astron. Lett.* **11**, 39.  
 Shitov, Yu. P., Malofeev, V. M. and Izvekova, V. A., 1988, *Sov. Astron. Lett.* **14**(3), 181.  
 Taylor, J. H., Manchester, R. N., and Lyne, A. G., 1993, *ApJS* **88**, 529.